

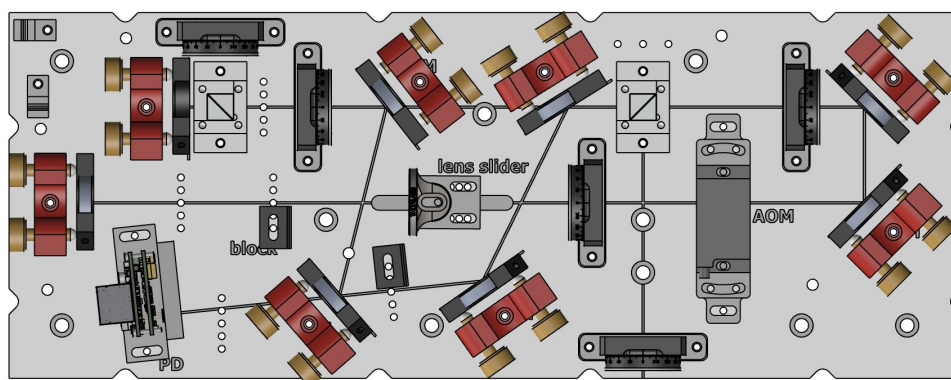
Design and setup of an acousto-optic modulator board in the double-pass configuration

Semester thesis as part of the physics Master of Science degree

Luca Ben Herrmann

Supervised by:

Martin Wagener, Moritz Fontboté Schmidt, Dr. Stephan Welte
& Prof. Dr. Jonathan Home



Trapped Ion Quantum Information Group
Institute for Quantum Electronics
ETH Zurich, Switzerland

March 2023

* Top picture: CAD Inventor design of the acousto-optic modulator board.

* Bottom picture: Laser beam diffracted into different orders by an acousto-optic modulator.

Abstract

Experiments using trapped ions or other atomic qubits require precise control over the frequency, phase and intensity of the many lasers used to manipulate, cool, readout and entangle the qubits. An acousto-optic modulator (AOM) can achieve MHz tunability of the laser frequency as well as control over the intensity and phase of the beam and is therefore widely used in such experiments. In this project two AOM setups in the single-pass and double-pass configuration were tested. In the single-pass configuration, a maximal diffraction efficiency of the first-order beam of 80 % was measured, whereas in the double-pass configuration a maximal diffraction efficiency of 58 % for the first-order beam was achieved. A rise-time of 113.8 ns with a delay of 400 ns was measured and the insertion loss of the AOM was measured to be of 6 %. Finally, a compact AOM board in the double-pass configuration was designed, manufactured and tested with fixed positions for all relevant optical and mechanical elements. The AOM board is suitable for a 19-inch rack system and multiple such boards can be placed in series to simplify the experimental setup of a trapped-ion experiment. A maximal diffraction efficiency of the first-order beam of 58 % was also measured on the AOM board in the double-pass configuration.

Acknowledgements

First of all, I would like to thank Martin Wagener, Moritz Fontboté Schmidt and Dr. Stephan Welte for supervising my project with great guidance, support and encouragement. Thank you for always being available to answer my questions and giving me feedback on my ideas as well as for teaching me new techniques and tools in the lab. Besides my project, it was exciting to learn about your work and the new setup. I thoroughly enjoyed working with all of you!

I would like to extend my gratitude to Prof. Jonathan Home for the opportunity to perform this semester project in his group and for taking the time to discuss my project in the weekly group meetings.

I would also like to thank Edgar Brucke for allowing me to use his previous CAD designs of the AOM boards for his setup at PSI and taking the time to help me improve my design.

Thank you Silvan Koch and Dr. Henry Fernandes Passagem for useful discussion regarding AOMs and how to maximise the diffraction efficiency.

Thank you Hendrik Timme and Leopold Konzett for great company in the crowded room B18.

Finally, I would like to thank everyone in the TIQI group for a friendly and motivating atmosphere with many interesting discussions!

Contents

1	Introduction	4
2	Theoretical background	5
2.1	Quantum information processing and the calcium ion	5
2.2	Acousto-optic modulators	5
2.3	Double-pass configuration of an acousto-optic modulator	7
3	Test setup	8
3.1	Characterization measurement of the AOM in the single-pass configuration	8
3.1.1	Rise time measurement	10
3.2	Characterization measurement of the AOM in the double-pass configuration	11
3.3	Guideline for setting up an acousto-optic modulator (AOM) in the double-pass configuration	14
4	Board design of the acousto-optic modulator (AOM) in the double-pass configuration	16
4.1	Measurement of the double-pass diffraction efficiency on the AOM breadboard	19
5	Conclusion	20
6	Bibliography	21
7	Appendix	23
7.1	Appendix A: Datasheets of the AOM	23
7.2	Appendix B: Beam profile	24

1 Introduction

In recent years the field of quantum information processing (QIP) has gained relevance and popularity due to the advancement of experimental techniques to control, manipulate and entangle the quantum states of multiple atoms, ions or other quantum systems as well as better theoretical understanding of such systems. The prospect of a large scale fault-tolerant quantum computer promises breakthrough advancements in many fields due to its speedup of certain computational tasks that are currently unfeasible to solve with a classical computer in a reasonable amount of time. For example, as shown by Shor [1], a fault-tolerant quantum computer could break RSA encryption exponentially faster than any classical computer.

Trapped ions are one of the leading platforms to build useful quantum devices. Ions can be trapped using electric fields in an ultra-high vacuum chamber [2, 3]. The ions, which take the role of the qubits in such an architecture, can then be cooled and controlled using lasers by targeting the different atomic transitions of the ion. By performing a series of operations on the qubits, computational tasks can be solved.

Typically in trapped-ion quantum computation, the quantum information is stored in the electronic degrees of freedom of the ion by choosing two of the energy levels as the $|0\rangle$ and $|1\rangle$ computational states [3, 2]. Quantum bits are subject to quantum decoherence which causes the loss of the information stored in the system and therefore limits the number of operation that can be performed before the system loses its information. One possibility to tackle this problem, is quantum error correction (QEC). An example of a QEC code is the surface code, where the information is redundantly encoded in multiple quantum bits providing an additional layer of protection against decoherence, and allowing for a correction of the errors once they are detected. Recently such a code was demonstrated with superconducting qubits [4].

An alternative route, which has seen remarkable progress in recent years, are bosonic QEC codes. A recent demonstration of the Gottesman-Kitaev-Preskill (GKP) code, which is an example of a bosonic QEC code [5], in a trapped-ion architecture was shown by the Trapped Ion Quantum Information group at ETH Zurich (TIQI) [6]. In this work the quantum information was encoded in the harmonic oscillator degrees of freedom of a single ion, which provides a higher-dimensional Hilbert space. In principle, such codes can provide a hardware-efficient implementation of QEC compared to the surface code where the quantum information is spread across multiple quantum bits.

A quantum computer based on trapped ions requires precise control over the lasers which are used to address different transition in the electronic structure of the ions. An acousto-optic modulator (AOM) is a device that allows control over the frequency, phase, and intensity of a laser beam.

In this project an acousto-optic modulator was tested in multiple setups and characterisation measurements of the AOM were performed. Furthermore, an AOM board in the double-pass configuration was designed using CAD, manufactured by the physics workshop at ETH Zurich and finally tested.

The aluminium AOM board consists of holes, extrusions and mounts, such that the optical and mechanical elements are placed in fixed positions. This can provide a more reliable configuration and can simplify alignment of the laser beam. The AOM board was designed to be suitable for a 19-inch rack system. Such racks are increasingly used in optical experiments since they allow for a more compact setup.

In the next section of this report (**chapter 2**) a short introduction to QIP experiments using trapped-ions will be given as well as an explanation of acousto-optic modulators. In **chapter 3** the characterisation measurements that were performed with the AOM in two different test setup, namely in the single-pass and double-pass configuration will be presented and discussed. Quantities such as the diffraction efficiency and the rise-time were measured and will be presented in this chapter. Finally, in **chapter 4** the CAD board design will be presented and the features of the design will be explained.

2 Theoretical background

In this section a brief introduction to quantum information processing using trapped ions will be presented, for a more detailed discussion of trapped-ion quantum information processing I refer the reader to [2, 3]. Additionally, the theory of acousto-optic modulators will be explained including a motivation for the double-pass configuration which was used extensively throughout this project. For an in-depth discussion of AOMs and the double-pass configuration I refer the reader to [7, 8, 9].

2.1 Quantum information processing and the calcium ion

Quantum information processing (QIP) using trapped ions typically uses the the electronic states of the ion to perform computations and store the quantum information [3]. For quantum computation, full control over the two-level system, i.e. the qubit, is necessary. Some of those computations include state preparation, readout of the qubit state and a universal set of gates. The Calcium ion $^{40}\text{Ca}^+$ is commonly used in trapped-ion experiments due to its simple level diagram which makes it a good two level system in which the qubit can be encoded. $^{40}\text{Ca}^+$ is an even isotope with no hyperfine structure due to the fact that it has 0 nuclear spin [3]. The level diagram is shown in Figure 1. For the $^{40}\text{Ca}^+$ ion the $|0\rangle$ state is defined in the S-manifold and the $|1\rangle$ state in the D-manifold of the electronic structure of the ion.

The various transitions of the ion are used for different operations. For example, the 397 nm dipole transition, for which the AOM will be tested, is used for Doppler cooling, electromagnetically Induced Transparency (EIT) cooling as well as for readout of the qubit state.

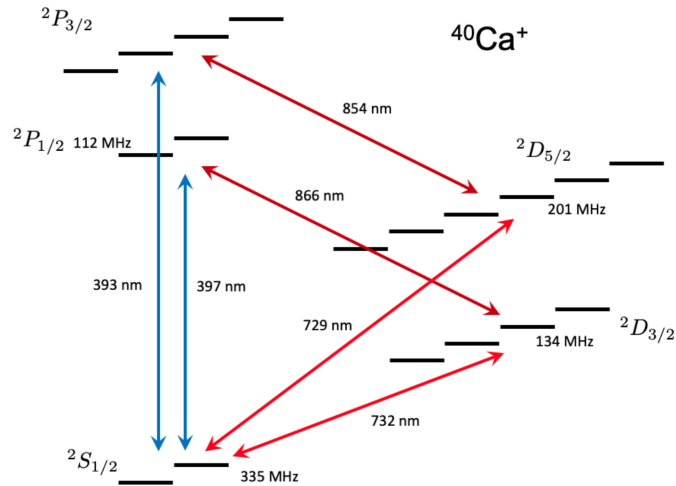


Figure 1: Level diagram of the $^{40}\text{Ca}^+$ ion at 119 G. The wavelengths needed to change the state of the ion are placed next to the corresponding arrows. Frequency numbers indicate the splitting of the manifolds in units of $\frac{\omega}{2\pi}$. The Figure was taken from [3].

2.2 Acousto-optic modulators

An acousto-optic modulator (AOM) consists of a piezoelectric transducer, which is driven with a radio frequency (RF) signal to create sound waves in a crystal or more generally a material made of glass or quartz [7]. In Figure 2 two sketches of an AOM are presented. The features of the AOM can be explained using the phonon-photon interaction that occurs between the sound waves in the crystal and the light that is incident on the AOM [8]. The frequency of the light is shifted by the frequency f_{RF} of the RF drive signal sent to the piezoelectric material times the diffraction order of the beam as follows: $f \rightarrow f + m \cdot f_{RF}$, where m is the diffraction order of the beam.

Using the Bragg diffraction the angle at which the different orders of the light are diffracted can be calculated:

$$2\Lambda \sin \theta = m \frac{\lambda}{n}$$

Where m is the order of the diffraction, λ is the wavelength of the incident light, Λ is the wavelength of the sound wave in the crystal, n is the refractive index of the crystal and θ is the angle of diffraction of the beam of order m [7]. The diffraction of the different orders can be seen in Figure 3. Besides modulating the frequency of the light as well as the diffraction angle of the diffracted beams, an AOM can also modulate the phase and the intensity of the beam as explained in [7, 8].

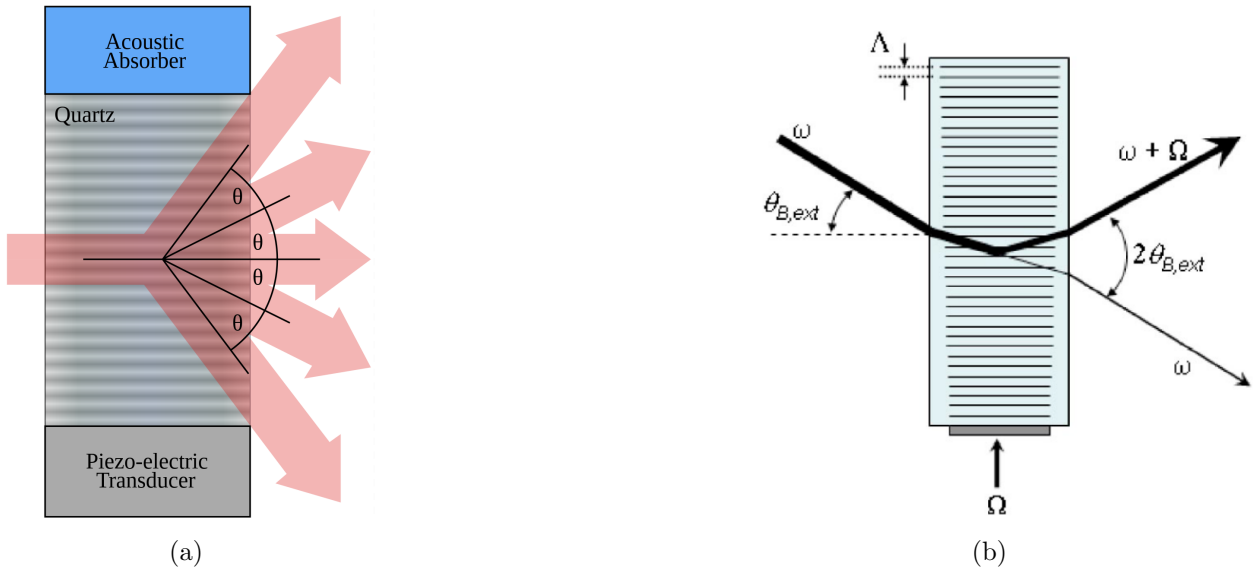


Figure 2: **a:** Sketch of an AOM consisting of a piezoelectric transducer that is driven with an RF signal to create sound waves in a quartz or crystal material, and thereby diffracts the light beam into several orders. Picture taken from [7]. **b:** Drawing of an AOM, taken from [8]. The beam is diffracted into the first-order, which is frequency shifted by the RF drive frequency Ω that is used to drive the AOM.

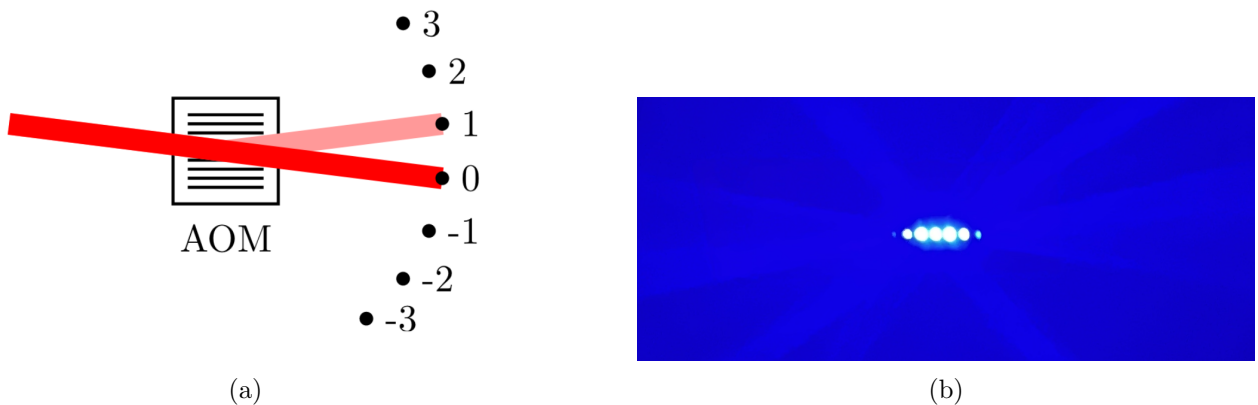


Figure 3: **a:** Laser beam diffracted into multiple order by an AOM. In this picture the RF drive is directed upwards in the AOM such that the first-order is position upwards of the zeroth order. The Figure was taken from [13] **b:** Picture taken from the experimental setup of the diffracted beams projected on a piece of paper. The picture was taken using a mobile phone camera.

2.3 Double-pass configuration of an acousto-optic modulator

There are two types of AOMs: free space and fibre-coupled. Fibre-coupled AOMs do not need any additional optical setup and only require the coupling of the laser into a fibre of the AOM. On the contrary, free space AOMs require an optical setup, such as the double-pass configuration to modulate the light and allow for frequency tunability of the drive frequency sent to the AOM. For a 397 nm laser, fibre-coupled AOMs are not suitable due to their low diffraction efficiencies for that wavelength regime. Therefore a free space AOM was used throughout this project.

The double-pass configuration is commonly used in optical experiments since it allows for easy tunability of the modulation frequency without having to adjust the setup. This is the main advantage of the double-pass configuration, where a scan over different modulation frequencies is possible because the double-passed beam is overlapped with the input beam irrespective of the diffraction angle [8, 9]. On the contrary, in the single-pass configuration the range of a frequency scan is limited because the diffraction angle is changed when scanning over different AOM drive frequencies. For the single-pass configuration the setup would need to be adjusted every time the AOM drive frequency is changed.

In the double-pass configuration the beam is first passed through the AOM where it is diffracted into multiple orders of diffraction. By using a mirror one can reflect the first-order diffraction beam back to the AOM, where it is diffracted again, such that the twice modulated beam can be overlapped with the input beam as shown in Figure 4. The modulated beam can be separated from the input beam by placing a quarter wave plate (QWP) between the AOM and the mirror as well as a polarization beam splitter (PBS) before the AOM. This will be shown in the next chapter in Figure 10. By passing through the QWP twice the linear polarization of the modulated beam is changed by 90° , such that the modulated beam can be separated from the input beam by the PBS. Furthermore, by placing a lens between the AOM and the mirror the RF drive frequency can be tuned without having to realign the setup since the lens ensures that the modulated beam is overlapped with the incoming beam irrespective of the deflection angle. The double-pass configuration including all elements is shown in Figures 9 and 10.

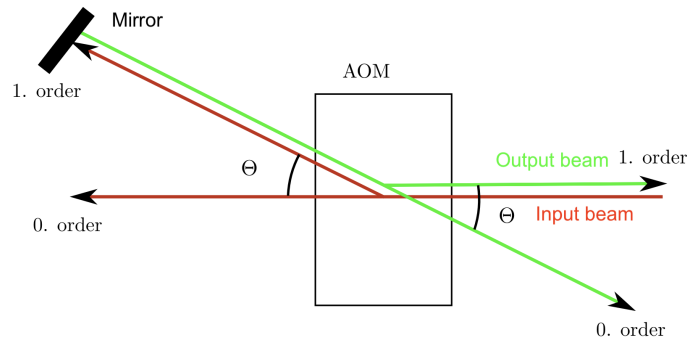


Figure 4: Sketch of the idea of the double-pass configuration of the AOM, taken and from [12] and additional labels were added. The input beam from the right side of the sketch (red) is diffracted by the AOM and the zeroth and first-order beam are shown. A mirror is placed to reflect the first-order beam back to the AOM, which causes the beam to diffract again. The first-order double-passed output beam (green) overlaps with the input beam. The advantage of the double-pass is that the beam which was modulated twice, is no longer dependent on the angle of the modulation, which depends on the RF drive frequency. This is achieved when a lens and a QWP are placed between the mirror and the AOM, and a PBS is placed before the AOM as shown in [9] and in Figure 10. Thereby the configuration allows changing the modulation frequency without having to realign the setup, which is a clear advantage over the single-pass configuration.

3 Test setup

The AOM that is currently being used for blue light in the TIQI group is by the manufacturer IntraAction. However, IntraAction is no longer delivering the required AOM and therefore a new AOM was needed. The AOM model used for this project was the **AOMO 3080-120 by Gooch & Housego** which has a 80 MHz center frequency. The specifications and characteristic device properties of this AOM were only tested for a wavelength range of 440 nm to 850 nm by the manufacturer. Since this device will be used for the 397 nm transition in the Ca40+ ion, it was necessary to perform characterization measurements of the AOM for the relevant wavelength. For the purpose of testing, a 401 nm laser was available with which all measurements were performed under the assumptions that the characteristic quantities and figures of merit of the AOM will be very similar for a 397 nm beam. The AOM is made of Tellurium dioxide (TeO₂) crystal which is nearly polarization independent. The diffraction efficiency as a function of the linear polarization of the beam was measured and a maximal variation of 2 % between the diffraction efficiency of two linear polarizations was found. This property plays an important role in the double-pass configuration, since it allows for a simpler configuration compared to when the AOM is polarization dependent (for example as it was shown in [11]). Previous projects with an AOM in the double-pass configuration were performed in the TIQI group. The reports of those projects [10, 11, 12, 13] were used for inspiration and for planning which measurements need to be performed.

Before measurements were performed the beam was first coupled to a single-mode fibre. After being emitted from the single-mode fibre, the beam profile was measured as shown in Figure 20 of the Appendix A2. From this measurement a Gaussian diameter of 793.8 μm and 831.3 μm , for the x and y direction respectively, were measured by the beam profiler. The collimator used to output coupling of the light from the fibre was chosen such that the beam diameter is smaller than 1 mm. This is important since the aperture of the AOM is 1 mm and the consequence of having a beam that is larger than the aperture of the AOM would be the loss of laser power as well as possible aberrations which would disrupt the characterization measurements.

An important specification of an AOM is its insertion loss. The insertion loss of an AOM is the percentage of laser power loss due to the beam passing through the AOM. Ideally the insertion loss should be minimal. The insertion loss is obtained by measuring the power of the laser beam before and after the beam passes through the AOM using a power meter. The insertion loss (in %) is then given by $L_{insertion} = 1 - \frac{Power_{after}}{Power_{before}}$ where $Power_{before}$ and $Power_{after}$ are the measured powers of the laser beam before and after the AOM. For the G&H AOM tested in this project, an **insertion loss of 5.4 %** was measured when the RF power signal sent to the AOM was turned off. When the RF power supply was turned on, an **insertion loss of 6.0 %** was measured. The power of the laser beam ($Power_{after}$) had to be measured very close after the AOM when the RF power was turned on, such that all orders of the diffracted beam are measured by the power meter.

In the next subsections the measurements of the AOM in the single and double-pass configuration will be presented and discussed. Possible uncertainties of the measurements were mostly due to the measurement devices and are not stated in the plots. In the last subsection a short guideline for setting up and aligning a double-pass configuration will be presented.

3.1 Characterization measurement of the AOM in the single-pass configuration

The first measurements were performed in the single-pass configuration. A sketch of the experimental setup using Inkspace and the Component Library by Alexander Franzen [14] can be seen in Figure 5 and a picture of the setup can be seen in Figure 6. This configuration is termed **single-pass** since the beam passes through the AOM one time. The AOM is driven using an RF signal generator which was connected to an amplifier to achieve sufficient drive powers. A 19.5 dBm directional coupler

(<https://www.minicircuits.com/pdfs/ZFDC-20-4+.pdf>) was used to measure the frequency of the RF signal using a spectrum analyser.

The beam was then passed through a QWP, half wave plate (HWP) and a PBS to obtain a linearly polarized beam. As explained in the previous chapter, when a beam is incident on the AOM at the right angle a diffraction pattern can be observed where the beam is diffracted into multiple orders. By placing the aperture in the correct position one can block all orders except the first-order which has a frequency equal to the initial frequency of the light plus the frequency of the RF signal that is sent to the AOM. This is the main use of the AOM, namely to shift the frequency of the beam. Typically either the first-order beam or the minus first-order beam is used for experiments, since for those diffraction orders a high diffraction efficiency can be achieved.

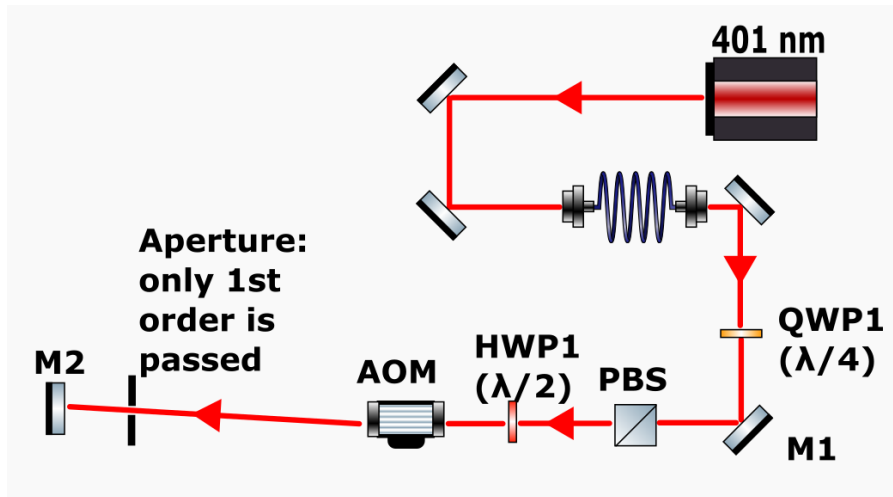


Figure 5: Inkspace picture of the test setup in the single-pass configuration, as it configured in the experiment shown in 6. The beam is first coupled into a single-mode fibre. Afterwards it is passed through a QWP to ensure the polarization is linear and not circular. Afterwards the beam passes through a PBS and a HWP before it enters the AOM. The beam is then diffracted by the AOM and only the first-order of the diffracted beam is passed through the aperture. In the measurements the power of the the first-order diffracted beam are performed after the aperture and before mirror M2.

The **diffraction efficiency** of the first-order beam is the ratio of the power of the first-order beam with respect to the power of the beam before it is diffracted by the AOM, i.e. the incident beam. A maximal diffraction efficiency is desirable. In Figure 7 plots of the diffraction efficiency of the first-order beam as a function of the AOM RF drive frequency and the AOM input power are shown. The **maximal diffraction efficiency of 80 %** is achieved at an RF frequency of 82 MHz and an AOM input power of 21.5 dBm.

The curve of the diffraction efficiency is very similar to the curves measured by the manufacturer for higher wavelengths as seen in the Appendix 1 in Figure 18. For the diffraction efficiency as a function of the AOM drive frequency for the frequencies between 70 and 80 MHz an unexpected pattern is observed. This is most likely due to slight misalignment of the aperture. For this measurement the aperture had to be realigned every time the frequency was changed, therefore it is possible that due to a small misalignment, the first-order beam was partially blocked by the aperture causing a lower diffraction efficiency for this frequency range. For the measurements in the double-pass configuration in Figure 11, where the aperture does not need to be realigned when changing the frequency, the diffraction efficiency followed a smoother pattern. This further hints that for the measurements of the diffraction efficiency in the single-pass configuration the aperture was slightly misaligned for the frequencies between 70 and 80 MHz.

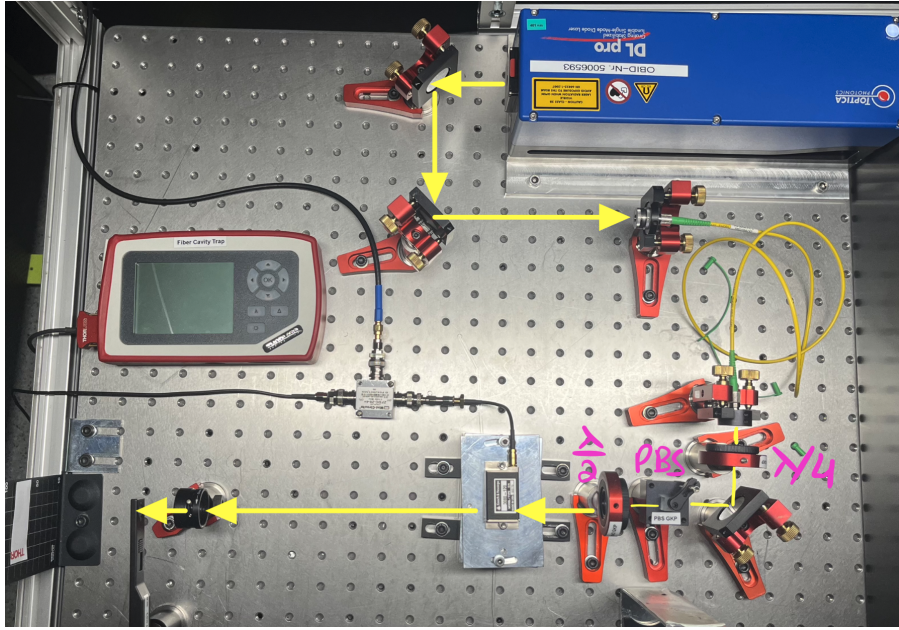


Figure 6: Test setup in the single-pass configuration. The different elements in the setup can be seen in a sketch of the setup in Figure 5

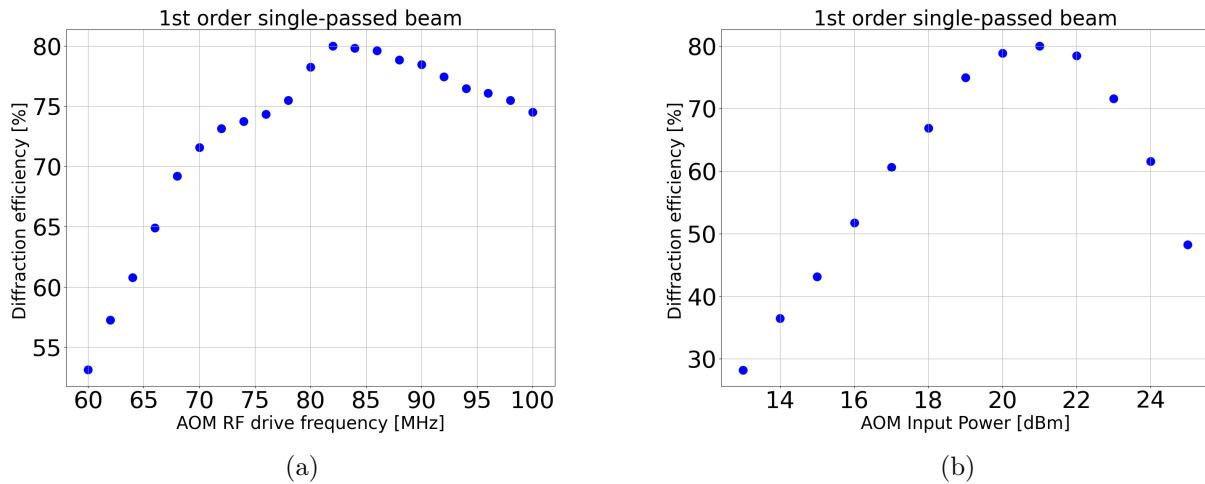


Figure 7: **a:** Plot of the diffraction efficiency of the first-order single-passed beam as a function of the RF drive frequency at an AOM input power of 21.5 dBm. The maximum diffraction efficiency of 80 % is achieved at 82 MHz. **b:** Plot of the diffraction efficiency of the first-order single-passed beam as a function of the AOM input power at an RF drive frequency of 80 MHz. The maximum diffraction efficiency of 80 % is achieved at 21 dBm.

3.1.1 Rise time measurement

Another crucial quantity of merit of an AOM is its rise-time. The rise time is defined as the time it takes the AOM to diffract the beam once the RF signal arrived in the AOM. For this measurement a Zaswa switch and an oscilloscope were used to trigger the RF signal sent to the AOM. The response of the beam which is modulated by the AOM is then monitored by a photodiode which is connected to the oscilloscope. In Figure 8 a screenshot of the measurement on oscilloscope is shown. A delay time between sending the signal to the RF source and the modulation of the beam by the AOM of 400 ns was measured. This delay can be compensated for by sending the RF drive 400 ns before the modulation of the beam by the AOM is needed. Furthermore, the rise time was measured at 118.3 ns.

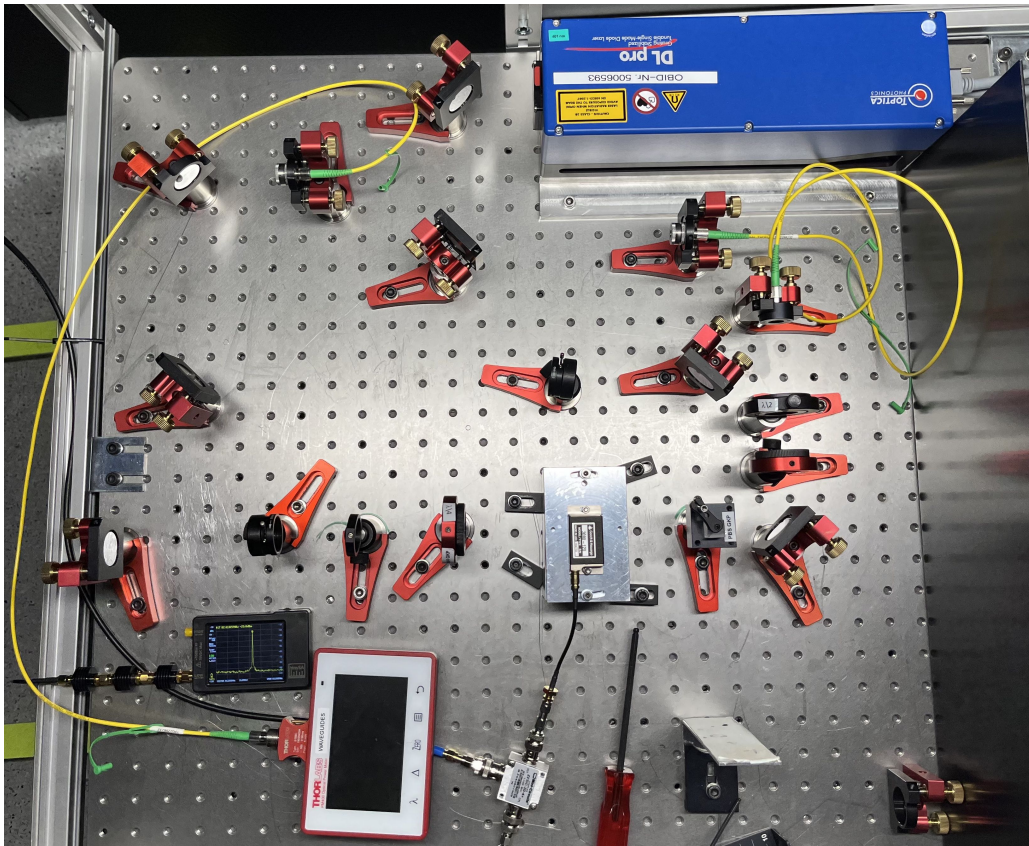


Figure 9: Experimental setup of the AOM in the double-pass configuration.

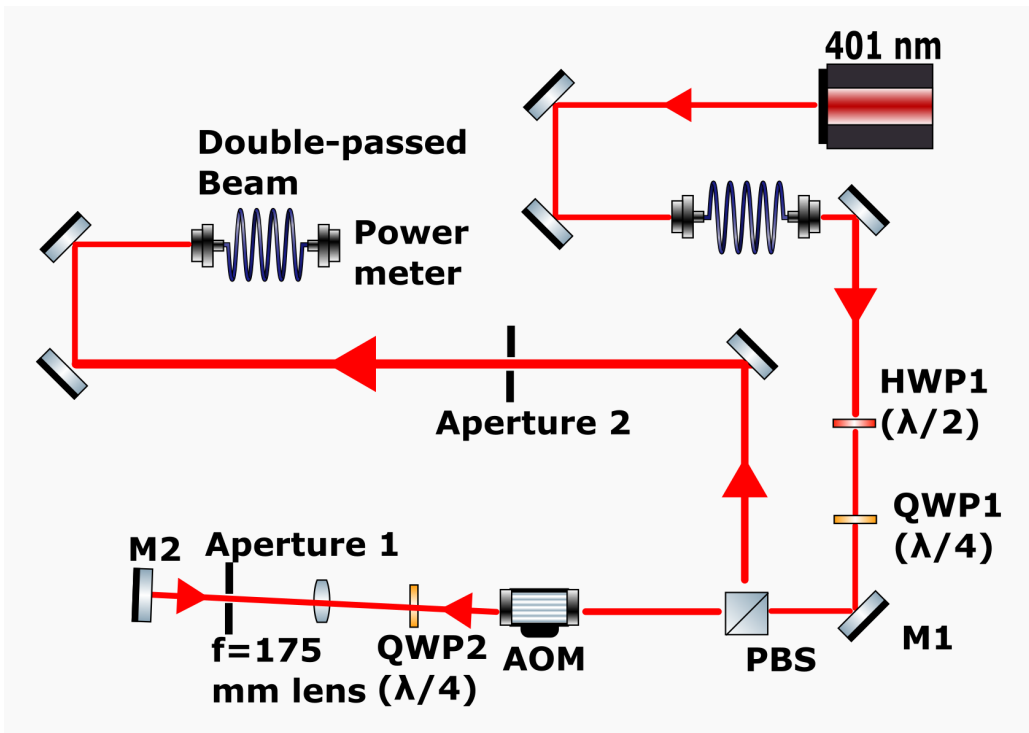
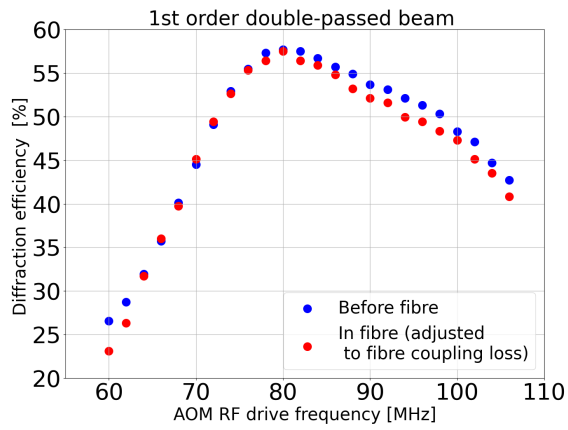
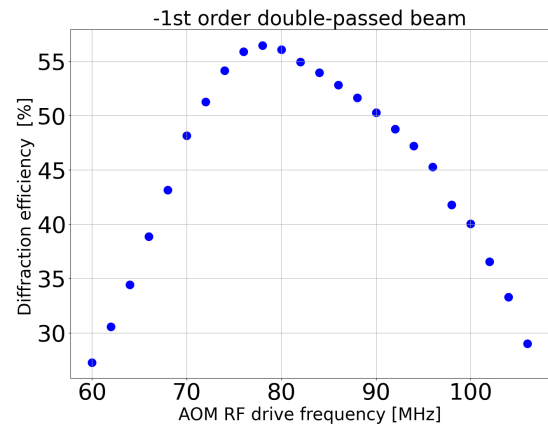


Figure 10: Inkspace picture of the test setup in the double-pass configuration.

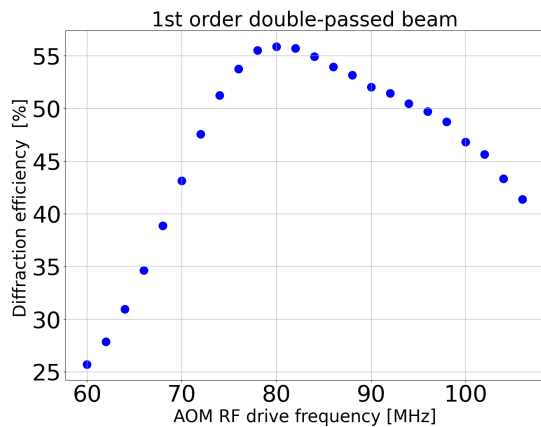


(a)

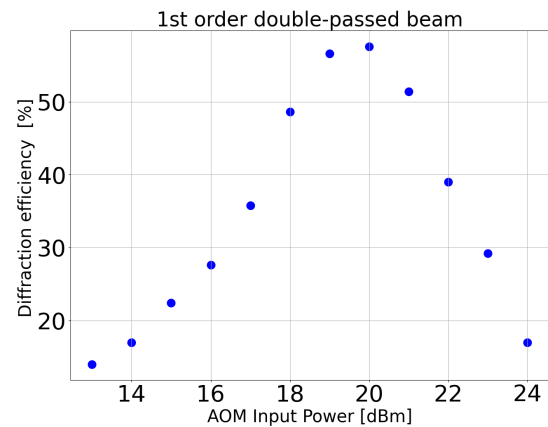


(b)

Figure 11: **a:** Plot of the diffraction efficiency of the first-order double-passed beam as a function of the RF drive frequency. Measurements of the light power were made before and after a fibre. The measurement of the intensity in the fibre was measured by coupling the beam into the fibre and connecting the fiber to a power meter with a suitable adapter. The loss of the fiber coupling was accounted for in the plot. This plot confirms that the double-pass configuration is indeed functional for different frequencies, without the need to realign the setup when changing the frequencies. The maximum diffraction efficiency of 58 % is achieved at 80 MHz. Throughout the measurements the AOM input power was set at 21.5 dBm. **b:** Plot of the diffraction efficiency of the minus-first-order double-passed beam as a function of the RF drive frequency. A maximal diffraction efficiency of 57 % is achieved at 80 MHz. Throughout the measurements AOM input power was set at 21.5 dBm.



(a)



(b)

Figure 12: **a:** Plot of the diffraction efficiency of the first-order double-passed beam as a function of the RF drive frequency. In this measurement a maximum diffraction efficiency of 56 % is achieved at 80 MHz. Throughout the measurements AOM input power was set at 21 dBm. In Figure 11.a slightly higher maximal diffraction efficiency of 58 % was found at a AOM input power of 21.5dBm. **b:** Plot of the diffraction efficiency of the first-order double-passed beam as a function of the AOM input power. The maximum diffraction efficiency of 57 % is achieved at 20 dBm. Throughout this measurements the frequency was set to 80 MHz.

3.3 Guideline for setting up an AOM in the double-pass configuration

Aligning an AOM in the double-pass configuration and optimizing the first-order diffraction efficiency can be a tedious and time-consuming task. After aligning the AOM multiple times throughout this project, I have found the following procedure to be the most efficient to maximize the diffraction efficiency of the first-order beam:

1. Align the beam into the aperture of the AOM and ensure that the insertion loss is minimised (for the tested AOM the insertion loss was minimised at 6%). This can be achieved by using the mirror M1 in 5 and the mount on which the single-mode fibre is placed and performing beam walking.
2. Adjust the beam line such that the beam height is constant while still observing that the insertion loss is minimal. This can be crucial since after optimising the single-pass diffraction efficiency, if the beam is not parallel to the plane of the board, it was difficult to achieve a high double-pass diffraction efficiency.
3. Now start optimising the first-order diffraction efficiency of the single-passed beam. For this begin without placing the lens between the AOM and the mirror. First place a card or a piece of paper where the diffracted beam is incident shortly before the mirror.
4. Change the angle of the AOM by rotating the mount until a diffraction pattern can be seen on the paper as shown in Figure 3. The diffraction efficiency of the first-order diffracted beam is typically maximized when there is a line cutting the zeroth-order beam. Adjust the angle of the AOM until this pattern is observable on the paper and ensure that the brightness of the first-order beam is maximal. Note that the direction of the first-order beam depends on which direction the RF drive signal is sent to the AOM. Now place a beam block or an aperture to block the zeroth-order and only pass the first-order beam.
5. To further optimize the diffraction efficiency of the first-order, perform beam walking in both the vertical and horizontal direction while making sure that the zeroth-order beam remains blocked and only the first-order beam is passed.
6. Adjust the RF drive frequency of the AOM as well as the power sent to the AOM to achieve a maximal diffraction efficiency. This concludes the alignment of the single-pass first-order beam.
7. Furthermore, I have found the following method useful for making sure that the zeroth-order beam is blocked: assuming the zeroth-order beam is blocked and the first-order beam is passed, once the RF drive is turned off the beam should be blocked. One can for example take a paper prior to the beam blocker and label where the first-order is located and when turning the RF drive off, the zeroth order beam should be exactly next to the noted position as well as in the corresponding direction depending on the RF drive.

After optimizing the diffraction efficiency of the single-passed beam, one can proceed with the optimization of the diffraction efficiency of the double-passed beam as follows:

1. Position the lens between the AOM and the mirror M2 in Figure 10 which reflects the beam back towards the AOM. When placing the lens ensure that the diffraction efficiency remains the same and that only the first-order beam is blocked. The distance between the AOM and the mirror M2 should equal the focal length of the lens as well as the distance between the lens and the mirror M2.
2. Place the QWP between the AOM and the lens.
3. Now the beam which is reflected by the mirror should be overlapped with the incoming beam. This can be achieved by adjusting the mirror and for example using a paper with a small hole such that the incoming beam is passed through the hole. If the beams are not overlapped the

reflected beam will be visible in a different position on the paper as the incoming beam and can be adjusted accordingly.

4. A diffraction pattern should be visible once the beams are overlapped and the first-order can be optimized as previously, while in addition the QWP needs to be adjusted such that the linear polarization of the beam is changed by 90° . Then, the output beam will be entirely reflected by the PBS which is positioned after the beam as it is shown in the sketch of the experimental setup in Figure 10.

Some of these procedures were adopted from reference [9] where a more comprehensive guide for the alignment of the double-pass configuration is introduced.

Additionally, throughout the project I have encountered the following issues which can cause problems in the alignment process and limit the maximal diffraction efficiency that can be achieved:

1. The mirrors, if sourced from Thorlabs, must have E01 or E02 coating to ensure the beam does not lose power after being reflected by the mirror (see Thorlabs website https://www.thorlabs.com/newgrouppage9.cfm?objectgroup_id=139 for the reflectance of the different coatings).
2. All optical elements such as the HWP, QWP and the PBS must be suitable for the desired wavelength, otherwise they might absorb a large percentage of the beam power and hence limit the diffraction efficiency.
3. Ensure that the lens is placed at exactly the specified focal length and that the distance from the AOM to the lens is equal to the distance from the lens to the mirror.
4. Ensure that the beam is collimated. Use a suitable collimator and check that the beam size should be smaller than the aperture, otherwise the diffraction efficiency is reduced and aberrations may occur.

4 Board design of the AOM in the double-pass configuration

The final part of the project consisted of the design of an aluminium AOM board. The AOM board includes holes, extrusions, mounts and other features such that all the optical and mechanical parts have a fixed position. This allows for a compact setup and simplifies the alignment of the beam due to the fixed positions of the elements. The design was made using the computer-aided design (CAD) software Inventor. A previous design of an AOM board designed by Edgar Brucke was used as a template and inspiration for the new design.

The board is designed such that it fits into a 19-inch rack system. Such systems are commonly used in experimental optics labs and are advantageous to organise the setup for an entire experiment. By placing the board in the rack system the experimental setup is simplified and can be separated from the main part of the experiment, for example the vacuum chamber where the ions are trapped. The idea is that one can simply couple the beam that was modulated by the AOM to a fibre and address the ions via the fibre which transports the modulated beam from the rack to the vacuum chamber. The AOM boards are easy to manufacture and offer a scaling advantage for experiments that require many laser beams.

The CAD model of the AOM board can be seen in Figure 13 and a picture of the manufactured board on Figure 15. The board was tested in a simpler configuration because some of the parts were not yet manufactured at the time the board was tested. The diffraction efficiency of the first-order beam in a double-pass configuration on the manufactured board is shown in Figure 17. The maximal diffraction efficiency of 58 % is reached at a RF drive frequency of 78 MHz and a AOM input power of 21.5 dBm. The achieved diffraction efficiency matches that of the test setup, thereby confirming that the design of the board satisfies its requirements. Besides the double-pass configuration on the board, there is a photodiode which can be used to monitor the power of the modulated beam by placing a mirror that transmits a small portion of the light, as shown in the bottom left part of the picture in Figure 13.

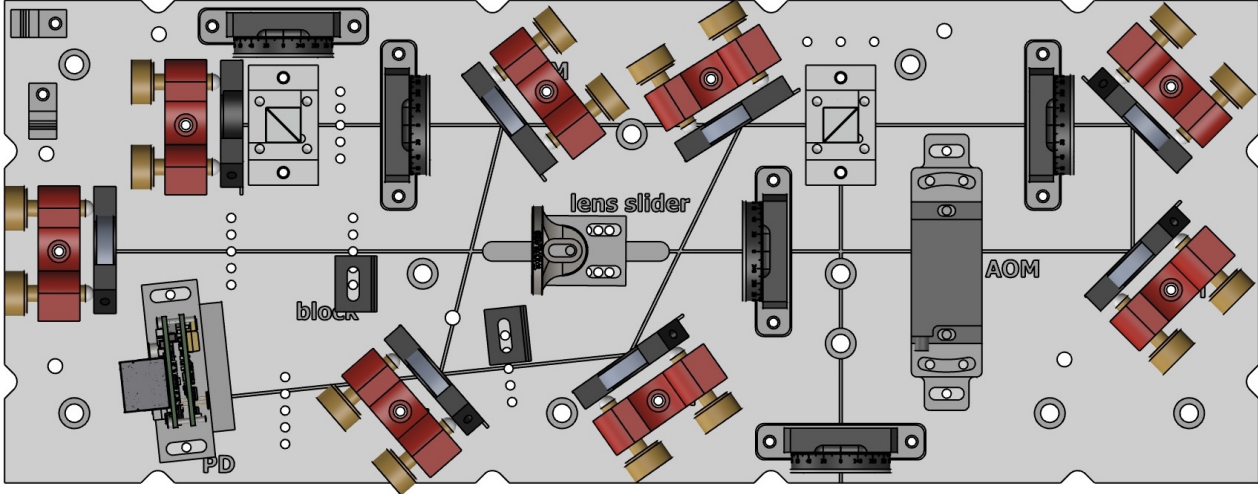


Figure 13: CAD model of an AOM board for a double-pass configuration setup including all the optics and mechanical elements. The board includes the necessary holes and extrusions such that the optical and mechanical elements have a fixed position. The AOM is mounted on a rotation mount. The model was designed using the CAD software Inventor.

In many trapped-ion experiments using Calcium $^{40}\text{Ca}^+$ ion, multiple 397 nm beams are used since the transition is used for different purposes, such as Doppler cooling, EIT cooling and state readout. Therefore, the AOM boards were designed such that multiple boards can be concatenated with only one input beam. Figure 14 shows a CAD model of 3 concatenated AOM boards. Furthermore an input board in the bottom right of Figure 14 can be seen. The input board consists of a mount where the collimator will be placed, a HWP and a mirror to input the beam into the main AOM boards. The

power of the input beam can be distributed over the different boards by adjusting the HWP which changes the linear polarisation of the beam and the PBS will reflect and transmit a certain percentage of the light depending on the polarisation chosen with the HWP.

On each board the beam is transmitted through the double-pass configuration. The double-passed beams are then overlapped using a combination of HWPs and PBSs before they can be coupled into a photonic-crystal fibre on the output board, as seen in the top left of Figure 14.

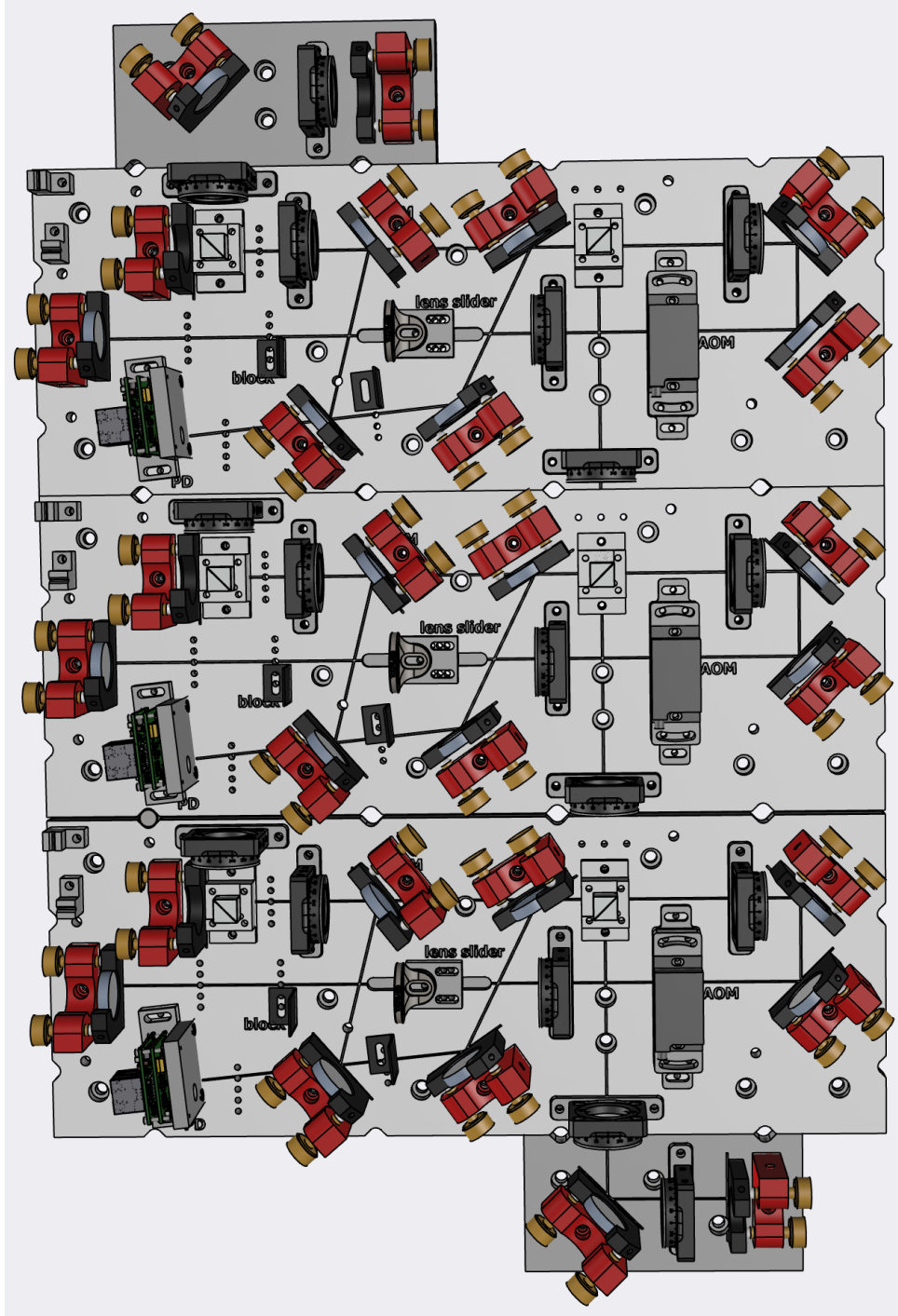


Figure 14: CAD model of 3 concatenated AOM boards and an input and output board. Such a configuration can be used to prepare multiple 397 nm beams using the AOM in the double-pass configuration which can then be used for different purposes.

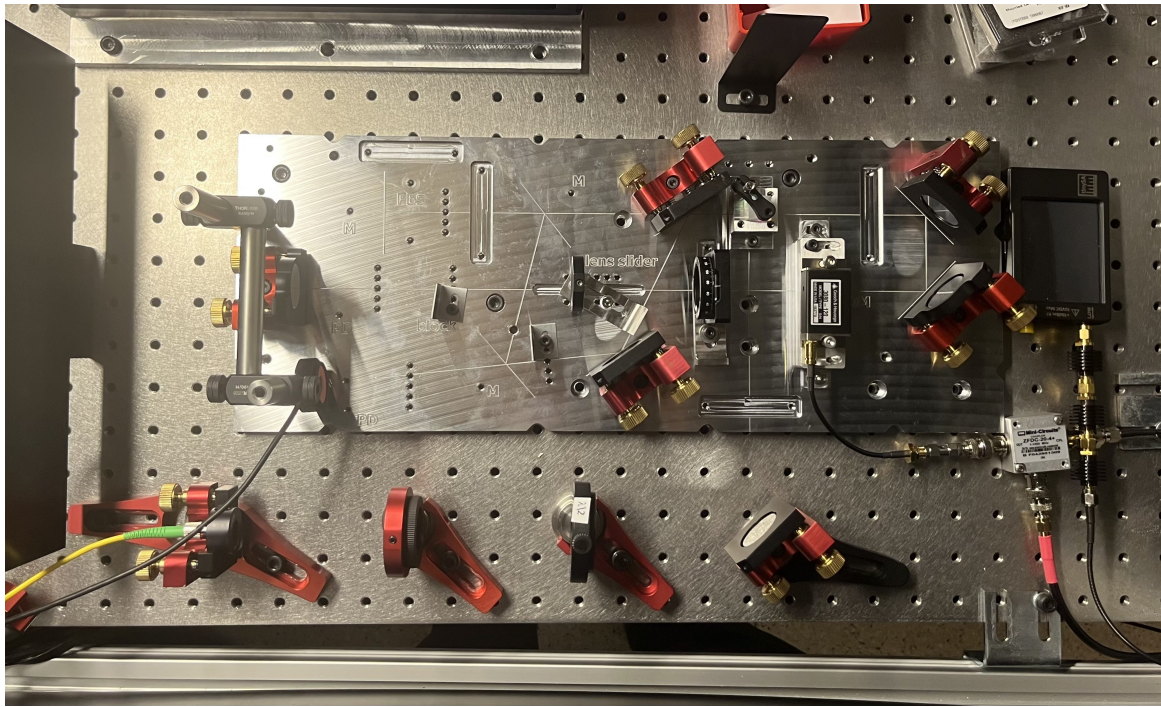


Figure 15: AOM board in the double-pass configuration. The board as well as other parts such as AOM rotation mount were manufactured by the ETH Zurich physics workshop. This configuration was used to test the AOM board and differs slightly from the CAD design of the board as shown in Figure 13 since at the time of testing the board, some of the parts were not yet manufactured

In Figure 16 a picture of the manufactured board can be seen. The board includes the necessary holes, extrusions for the mount and the beamline as well as labels of where the optical or mechanical elements are to be placed. The CAD files can be found on the following folder of the TIQI group in the J drive, which is accessible only to members of the group: *J:\ Projects\GKP_Gates\Hardware_Projects\HPR020 Luca AOM Board\397_board - modified by Luca - Final folder\AOM Board - Luca - new design.*

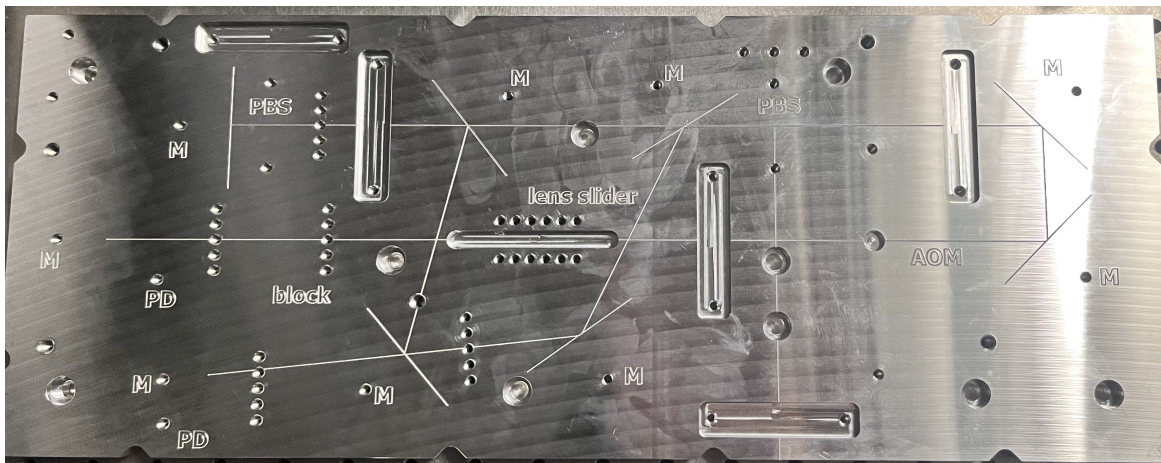


Figure 16: Picture of the manufactured AOM board by the ETH Zurich physics workshop.

4.1 Measurement of the double-pass diffraction efficiency on the AOM breadboard

The diffraction efficiency of the first-order double-passed beam is shown in Figure 17. A maximal diffraction efficiency of 58 % was achieved. The diffraction efficiency on the AOM board was therefore equivalent to what was measured on the test setup. On the test setup, as shown in Figure 9, an aperture was used to block the unwanted diffraction orders, whereas on the AOM board a beam block is used. Besides this difference, the measurements were performed with the same laser, RF source and optics that were used in the test setup. In Figure 15 a picture of the setup used to test the board and perform the measurements of the diffraction efficiency on the AOM board is shown.

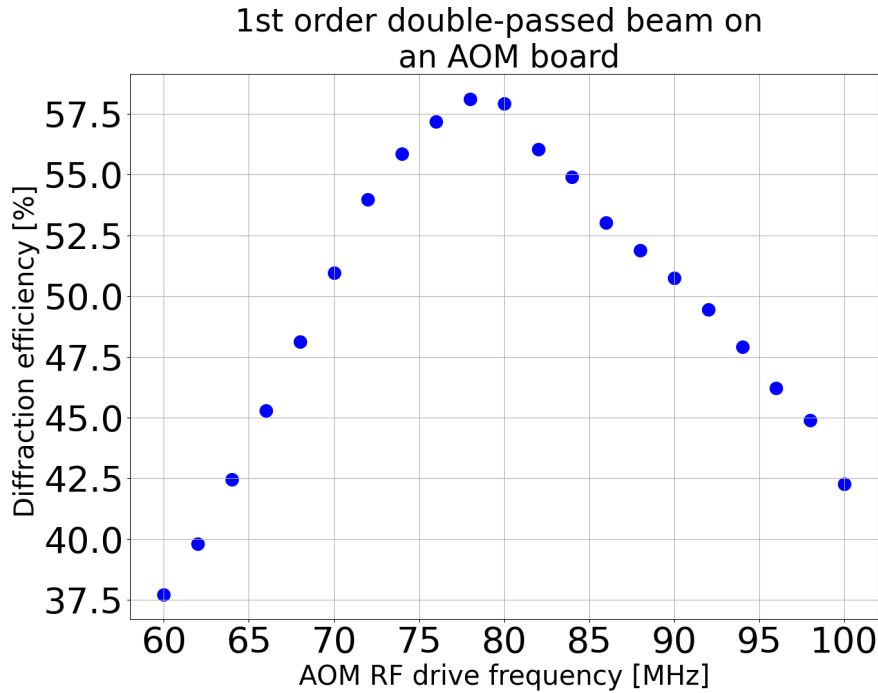


Figure 17: Diffraction efficiency of the first-order double-passed beam on the AOM board as shown in Figure 15. A maximum diffraction efficiency of 58 % can be achieved at a drive frequency of 78 MHz and a an AOM input power of 21.5 dBm.

5 Conclusion

Throughout this project the characteristic properties of the G&H AOM were tested for UV light, namely for a 401nm wavelength beam. The results confirm that the AOM can be used slightly outside of its specified wavelength range of 440-850 nm. A maximal single-pass diffraction efficiency of 80 % was measured for the first-order beam. The insertion loss of the AOM was found to be of 6.0% when the AOM was supplied with the required RF signal. A rise time of 113.8 ns was measured with a response delay of 400 ns. Most importantly, the double-pass diffraction efficiency of the first-order beam was found to be 58 % at the optimal parameters, making the AOM suitable for trapped-ion experiments.

Additionally, a CAD model of an AOM board with holes, extrusions and additional mounts which fixes the position of the optical and mechanical elements for a double-pass configuration was designed and manufactured. Such a board offers a compact design and ease of alignment due to the fixed position of all the elements. The double-pass diffraction efficiency of the first-order beam was also tested on the board and measured at a maximum of 58 %. The AOM board is compatible for a 19-inch rack system. Furthermore, the board was designed such that multiple boards can be concatenated after each other with only a single input beam being split across the different boards and later collected by overlapping the modulated beams. This feature is advantageous since in many trapped-ion experiments multiple beams for the 397 nm transition of the $^{40}\text{Ca}^+$ ion are needed. Those beams should be modulated with different frequencies, sometimes with different AOMs with the correspondingly required center frequency, which depends on the purpose for which the beam will be used in the experiment.

In the future, the parts which were not yet manufactured when the final measurements with the AOM board were performed are still to be tested. Namely the waveplate mounts, the photodiode and the lens slider. Furthermore, the concatenation of multiple boards with multiple modulated output beams needs to be tested.

In conclusion, optical experiments require precise control over the lasers which are used to perform operations on the quantum system. Acousto-optic modulators are commonly used in such experiments to control the properties of the light. The board designed in this project allows for quicker and more scalable control of many laser beams.

6 Bibliography

- [1] Peter W. Shor. "Polynomial-Time Algorithms for Prime Factorization and Discrete Logarithms on a Quantum Computer". *SIAM Journal on Computing* 26.5, August 1995. Arxiv link: <https://arxiv.org/abs/quant-ph/9508027>.
- [2] Roei Ozeri. "Tutorial: The Trapped-Ion Qubit Toolbox". *Contemporary Physics* 52, no. 6 :pages 531 to 550, November 2011. <https://doi.org/10.1080/00107514.2011.603578>.
- [3] Kienzler Daniel. "Trapped Ion Physics". Lecture notes, February 2022.
- [4] Sebastian Krinner et al. "Realizing Repeated Quantum Error Correction in a Distance-Three Surface Code". arXiv: 2112.03708, December 2021. <http://arxiv.org/abs/2112.03708>.
- [5] Moritz Fontboté Schmidt. "Towards Improved Control of Grid States in Motional States of Trapped Ions". Master's thesis, ETH Zurich, May 2022.
- [6] Christa Flühmann, Thanh Long Nguyen, Matteo Marinelli, Vlad Negnevitsky, Karan Mehta, and Jonathan Home. "Encoding a Qubit in a Trapped-Ion Mechanical Oscillator". *Nature* 566 (7745): 513-517, 2019. <https://doi.org/10.1038/s41586-019-0960-6>.
- [7] "Acousto-Optic Modulator In Wikipedia", June 2022. https://en.wikipedia.org/w/index.php?title=Acousto-optic_modulator&oldid=1094640241.
- [8] E. A. Donley, T. P. Heavner, F. Levi, M. O. Tataw, and S. R. Jefferts. "Double-Pass Acousto-Optic Modulator System". *Review of Scientific Instruments* 76, no. 6: 063112, June 2005. <https://doi.org/10.1063/1.1930095>
- [9] D. J. McCarron. "A Guide to Acousto-Optic Modulators", December 2007. https://www.researchgate.net/publication/242324156_A_Guide_to_Acousto-Optic_Modulators
- [10] Lukas Möller, "Set up of a double-pass AOM system for an ion trap experiment". Semester project in the TIQI group, October 2018. https://ethz.ch/content/dam/ethz/special-interest/phys/quantum-electronics/tiqi-dam/documents/semester_theses/semesterproject-Lukas-Moeller.
- [11] Lukas Möller. "Light delivery and imaging for the cavity-integrated trap experiment". Project in the TIQI group, 2018.
- [12] Chanson, Mathieu. "Design of a Stable AOM Double-Pass Setup for Trapped-Ion Laser Systems". Project in the TIQI group, October 2012. https://ethz.ch/content/dam/ethz/special-interest/phys/quantum-electronics/tiqi-dam/documents/semester_theses/semesterthesis-mathieu_chanson.pdf.
- [13] Doruk Efe Gokmen. "Optical Design for Gaussian Beam Elliptical Spot Shaping & AOM Double-pass Configuration for Realising Calcium Ion Thermal Qubit". Semester project in the TIQI group, September 2017. https://ethz.ch/content/dam/ethz/special-interest/phys/quantum-electronics/tiqi-dam/documents/semester_theses/semesterthesis-Doruk.
- [14] Alexander Franzen. Component library. <http://www.gwoptics.org/ComponentLibrary/>.

Acronyms

AOM acousto-optic modulator	4–11, 14, 16, 20
CAD computer-aided design	16
EIT electromagnetically Induced Transparency	5, 16
GKP Gottesman-Kitaev-Preskill	4
HWP half wave plate	9, 11, 15 ff.
PBS polarization beam splitter	7, 9, 11, 15, 17
QEC quantum error correction	4
QIP quantum information processing	4 f.
QWP quarter wave plate	7, 9, 11, 14 f.
RF radio frequency	5, 7–11, 16, 19
TIQI Trapped Ion Quantum Information group at ETH Zurich	4, 8, 18

7 Appendix

7.1 Appendix A: Datasheets of the AOM

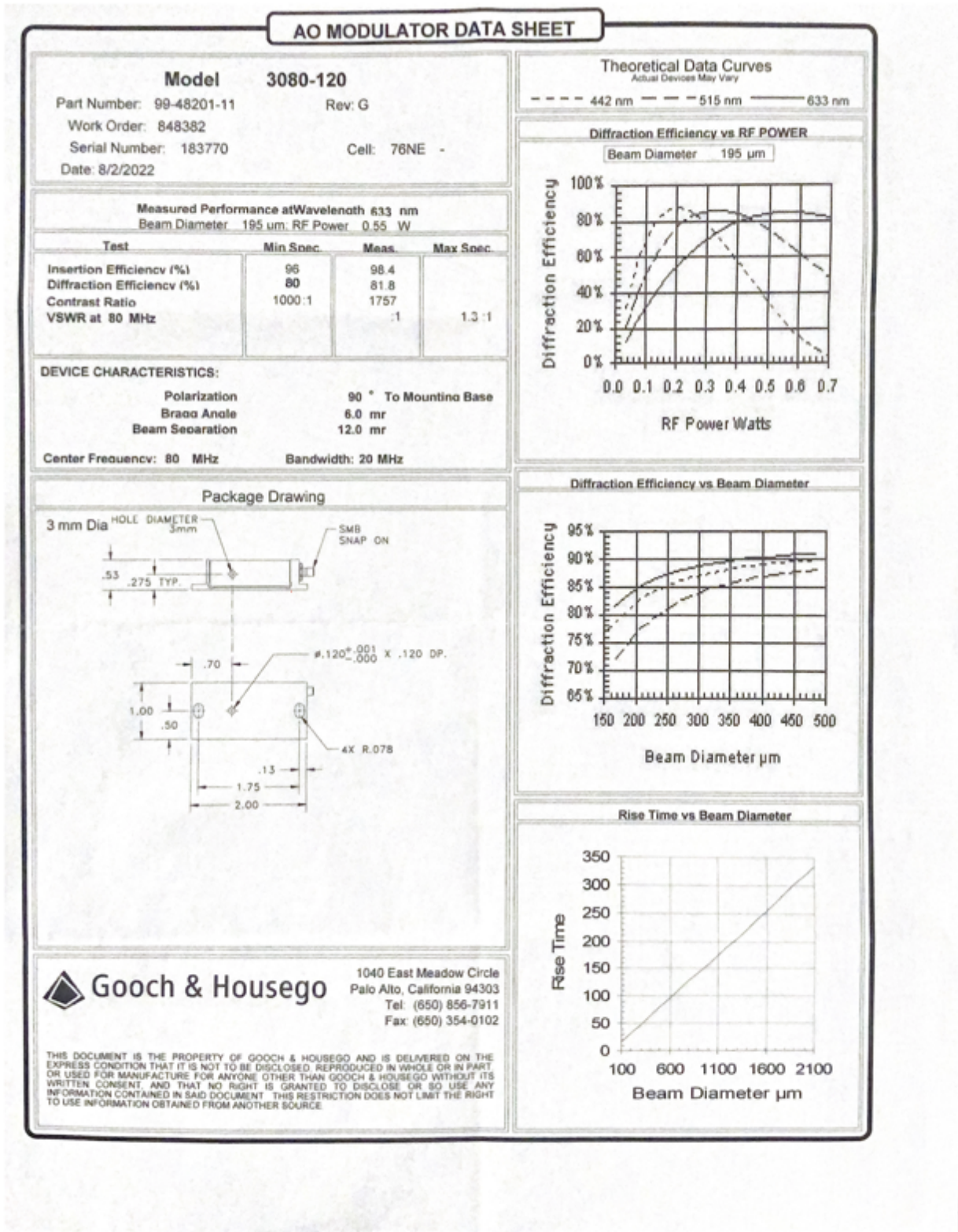


Figure 18: Datasheet of the AOM which was supplied with the shipment of the AOM

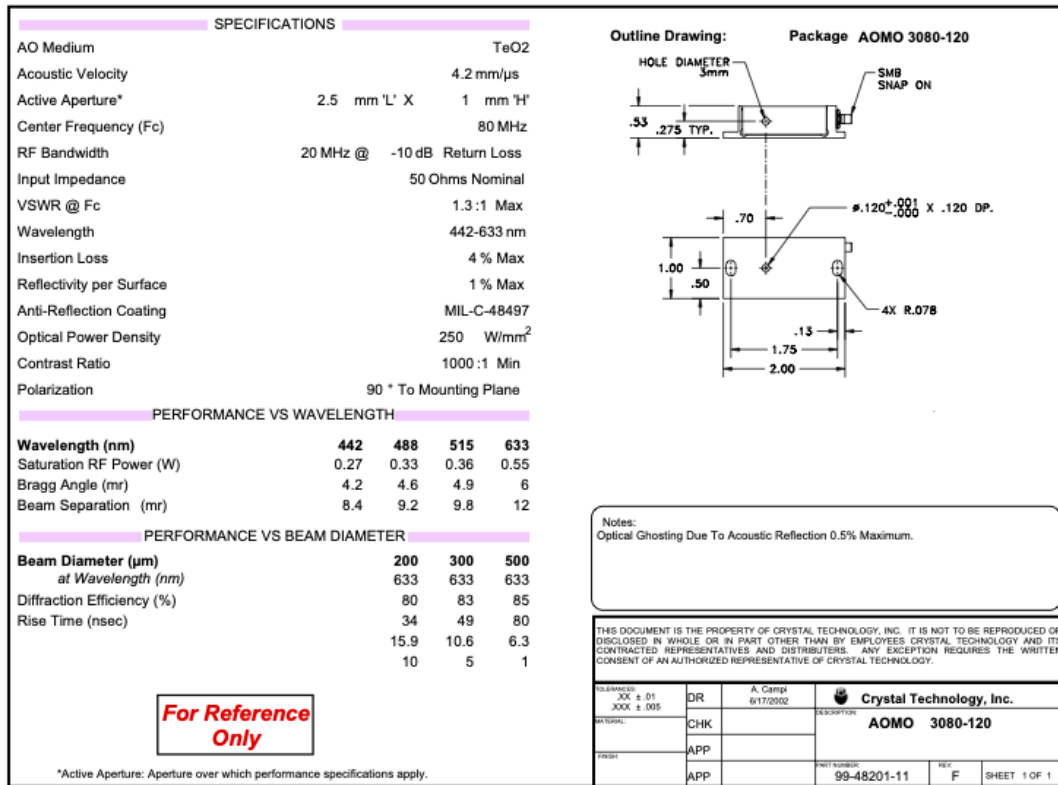


Figure 19: Datasheet of the AOM used in this project as found in the website <https://gandh.com/products/acousto-optics/modulators/aomo-3080-120>

7.2 Appendix B: Beam profile

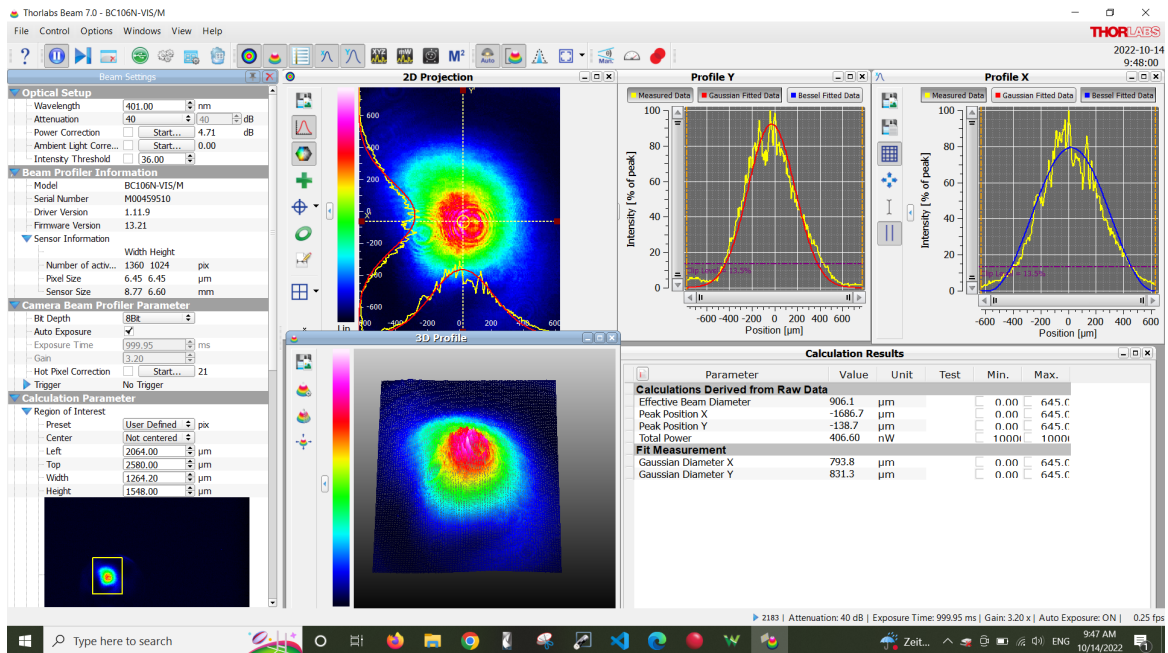


Figure 20: Beam profile measurement of the 401 nm laser beam after it is emitted from a single-mode fibre.